Multivariate recurrence network analysis for characterizing horizontal oil-water two-phase flow

Zhong-Ke Gao,[1,2,3] Xin-Wang Zhang,[1] Ning-De Jin,[1,*] Norbert Marwan,[3] and Jürgen Kurths[2,3,4]
[1]*School of Electrical Engineering and Automation, Tianjin University, Tianjin 300072, China*
[2]*Department of Physics, Humboldt University, Berlin 12489, Germany*
[3]*Potsdam Institute for Climate Impact Research, Potsdam 14473, Germany*
[4]*Institute for Complex Systems and Mathematical Biology, University of Aberdeen, Aberdeen, Scotland AB24 3UE, United Kingdom*
(Received 2 May 2013; revised manuscript received 1 July 2013; published 13 September 2013)

Characterizing complex patterns arising from horizontal oil-water two-phase flows is a contemporary and challenging problem of paramount importance. We design a new multisector conductance sensor and systematically carry out horizontal oil-water two-phase flow experiments for measuring multivariate signals of different flow patterns. We then infer multivariate recurrence networks from these experimental data and investigate local cross-network properties for each constructed network. Our results demonstrate that a cross-clustering coefficient from a multivariate recurrence network is very sensitive to transitions among different flow patterns and recovers quantitative insights into the flow behavior underlying horizontal oil-water flows. These properties render multivariate recurrence networks particularly powerful for investigating a horizontal oil-water two-phase flow system and its complex interacting components from a network perspective.

DOI: 10.1103/PhysRevE.88.032910 PACS number(s): 05.45.Tp, 47.55.−t, 89.75.Fb

I. INTRODUCTION

Horizontal oil-water two-phase flow is common in a diverse range of industrial processes and particularly in the petroleum industry, where a mixture of oil and water often flows through pipes for long distances for production and usage. The investigations of horizontal oil-water flows are of great importance, especially for the prediction of pressure drop in the horizontal oil wells, measurement of flow parameters, and optimization of industrial production process. However, despite its importance, horizontal oil-water flows have not been explored as intensively as gas-liquid flows. An important aspect of the study of a two-phase flow is a characterization of flow patterns. A flow pattern is the shape and spatial distribution of the two-phase flow within the pipe. The interest in flow patterns lies in the fact that in each pattern the flow has certain hydrodynamic characteristics. Up to now, the dynamical mechanisms leading to the formation of various patterns in horizontal oil-water flows have been elusive.

The exploration of horizontal oil-water two-phase flow has attracted much attention from physical and chemical research fields on account of its significant importance. Trallero *et al.* [1] experimentally investigated horizontal oil-water two-phase flow in a 50.8-mm-inner-diameter (ID) pipe and classified the horizontal oil-water flow patterns into *segregated flow* and *dispersed flow*, in which the segregated flow includes (1) a stratified flow pattern (ST) and (2) a stratified flow with mixing at interface pattern (ST and MI); the dispersed flow includes (3) a dispersion of oil in water and water flow pattern (D O-in-W and W), (4) a dispersion of water in oil and oil in water flow pattern (D W-in-O and D O-in-W), (5) a dispersion of oil in water flow pattern (D O-in-W), and (6) a dispersion of water in oil flow pattern (D W-in-O). Angeli and Hewitt [2] combined directed observation with conductance probes measurements to experimentally identify different horizontal oil-water flow patterns. By using numerical simulations and analytical solutions, Ng *et al.* [3] predicted the boundary shape of a stratified flow. Brauner and Ullmann [4] experimentally investigated the flow structure and interface shape of the horizontal oil-water two-phase flow. By using a probability density function analysis and the wavelet multiresolution technique, Chakrabarti *et al.* [5] studied the transition from a water continuous to an oil continuous flow pattern in a horizontal pipe. Piela *et al.* [6] conducted experiments to study the phase inversion behavior of horizontal oil-water flows. Kumara *et al.* [7] employed the particle image velocimetry technique to characterize the flow structure of oil-water flows in a horizontal pipe. Al-Wahaibi and Angeli [8,9] made an experimental investigation on the transition from a horizontal oil-water stratified flow to a nonstratified flow and also experimentally studied the interfacial waves in stratified horizontal oil-water flows. By using laser-induced fluorescence, Morgan *et al.* [10] investigated the horizontal liquid-liquid flow characteristics at low superficial velocities.

Despite the existing results, there still exist significant challenges in the study of horizontal oil-water two-phase flow. In particular, how to characterize the dynamic flow behavior underlying horizontal oil-water flow patterns from experimental measurements is an as yet unsolved problem. We note that, although the approaches of nonlinear time series analysis such as the complexity measure [11] and time-frequency representation [12] have been successfully used to distinguish gas-liquid flow patterns [13], these approaches have severe limitations as applied to the investigation of horizontal oil-water flow patterns, mainly due to the fact that there exist intrinsic differences in the physics of the two flow situations and there is no guarantee that the information available for gas-liquid flows can be extended to horizontal liquid-liquid systems. In addition, for the multivariate time series analysis, correlation analysis is usually infeasible to effectively identify and characterize the horizontal oil-water flow patterns, as we will show. In this regard, characterizing complex patterns arising from horizontal oil-water two-phase flow is a challenging problem of significant interest.

*Corresponding author: ndjin@tju.edu.cn

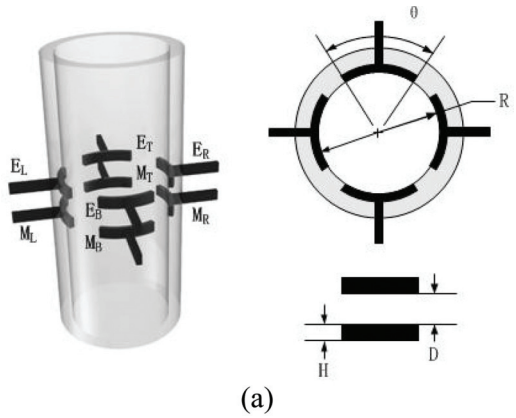

(a)

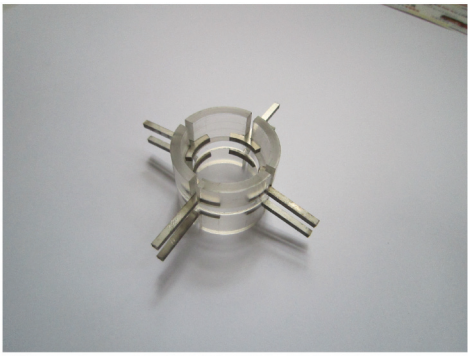

(b)

FIG. 1. (Color online) Structure of the four-sector conductance sensor.

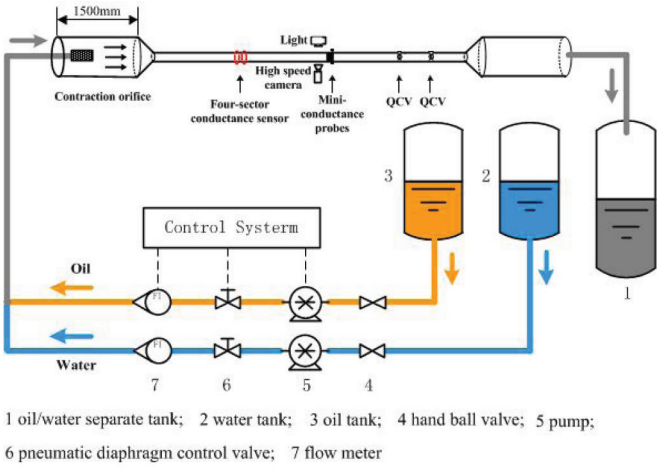

(a)

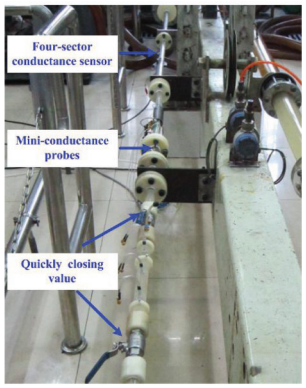

(b)

FIG. 2. (Color online) Experimental flow loop facility.

Complex network theory has undergone a strong development in the last decade and has contributed significantly to our understanding of complex systems [14–25]. Recently, a variety of approaches has been proposed for investigating time series by means of complex network approaches [26–31], such as approaches based on the concept of quasiperiodic cycle [26,27], correlations [28], visibility [29–31], classical multidimensional scaling [32], and recurrence analysis (phase-space reconstruction) [33–41]. Complex network analysis of time series has been successfully applied in many research fields, such as network topology estimation [42,43], financial system [44,45], climate [46,47], human gait [48], human brain [49], genomics [50], human ventricular fibrillation [51], multiphase flow system [52,53], grain property networks [54,55], and friction networks in nucleation processes [56,57]. As a particularly useful example, recurrence networks [33–41] provide a widely applicable novel tool that has already proven its great potential for geometrically studying complex dynamical systems and time series. Bridging time series analysis and complex networks can be an appealing approach for experimental data analysis. In this paper, we design a new multisector conductance sensor and systematically carry out horizontal oil-water two-phase flow experiments for measuring multivariate signals of different flow patterns. Based on the recently proposed multivariate extensions of recurrence networks [58], we infer and analyze multivariate recurrence networks from our experimental data, and our results suggest that the multivariate recurrence network can be a particularly powerful tool for investigating flow behavior underlying horizontal oil-water two-phase flow.

II. EXPERIMENTS AND DATA ACQUISITION

The horizontal oil-water two-phase flow experiment in a 20 mm-inner-diameter (ID) pipe was carried out in the multiphase flow loop at Tianjin University. The experimental media are tap water and no. 15 industry white oil with a viscosity of 11.984 mPa s (40 °C) and a surface tension of 0.035 N/m. In order to measure the local flow behavior of horizontal oil-water flows, we design a new four-sector conductance sensor, as shown in Fig. 1. It consists of eight alloy titanium concave electrodes axially separated and flush mounted on the inside wall of the flowing pipe. E_T, E_R, E_B, and E_L are exciting electrodes, and M_T, M_R, M_B, and M_L are measuring electrodes. The representing geometric parameters of the sensor are defined as follows: the exciting and measuring electrode angle θ, the electrode height H, the inner pipe radius R, the distance between the exciting and the measuring electrode D. The sectors M_A, M_B, M_C, and M_D of the sensor enable us to measure the local flow behavior in the top, right, bottom, and left part of the horizontal pipe, respectively. The measurement system consists of several parts: a four-sector conductance sensor, miniconductance probes, a high-speed video camera recorder, an exciting-signal generating circuit, a signal modulating module, a data-acquisition device

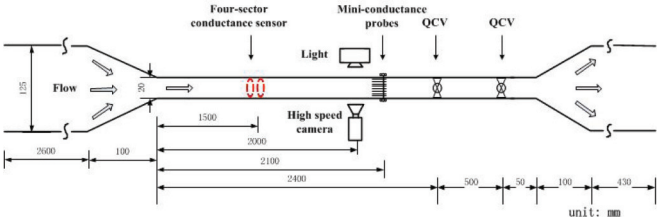

FIG. 3. (Color online) Scheme of the sensor system installed in the 20-mm-ID pipe.

(PXI 4472 and 6115 card, National Instruments), and a software for preliminary signal processing. In our experiment, we concentrated the oil-water flows from a 125-mm-ID pipe into a 20-mm-ID pipe by using an umbrella-shape bell mouth to generate a high oil and water flow rate. Figure 2 shows our experimental flow loop facility. The axial length of the 20-mm-ID pipe is 2.95 m, and all the conductance sensors are installed in the 20-mm-ID pipe. Figure 3 shows the scheme of the sensor system installed in the 20-mm-ID pipe.

A typical experimental run starts by generating a water flow at a fixed rate in the pipe and then gradually increasing the oil flow rate. When the water and oil flow rates reach a predefined ratio, a certain flow condition is obtained and conductance fluctuating signals are then acquired from the four-sector conductance sensor and miniconductance probes. The high-speed video camera recorder and the miniconductance probes signals are mainly used for defining different horizontal oil-water flow patterns. In our experiment, the oil and water superficial velocities are both in the range of 0.1–3 m/s. Based on the flow pattern definition proposed by Trallero *et al.* [1], we have observed six different horizontal oil-water flow patterns in the experiment, as shown in Fig. 4, i.e., ST flow pattern, ST and MI flow pattern, D O-in-W and W flow pattern, D W-in-O and D O-in-W flow pattern, D O-in-W flow pattern, and D W-in-O flow pattern. Since the D W-in-O flow pattern is totally nonconductive, we focus our research on five conductive flow patterns. The flow signals from the four-sector conductance sensor corresponding to the five conductive flow patterns are shown in Fig. 5, where U_{so} and U_{sw} represent the oil superficial velocity and the water superficial velocity, respectively.

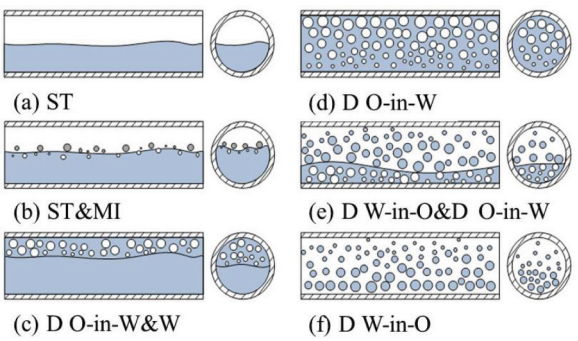

FIG. 4. (Color online) Experimentally observed horizontal oil-water flow patterns.

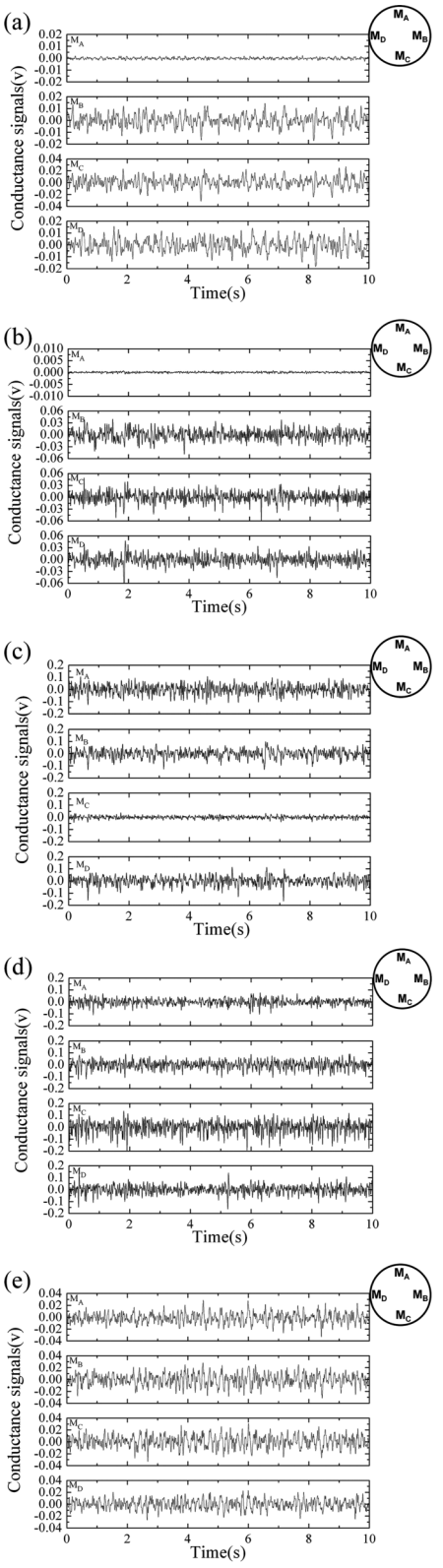

FIG. 5. The signals from the four-sector conductance sensor for different horizontal oil-water flow patterns. (a) ST flow ($U_{sw} = 0.1105$ m/s, $U_{so} = 0.1326$ m/s). (b) ST and MI flow ($U_{sw} = 0.2210$ m/s, $U_{so} = 0.1945$ m/s). (c) D O-in-W and W flow ($U_{sw} = 0.7368$ m/s, $U_{so} = 0.1945$ m/s). (d) D W-in-O and D O-in-W flow ($U_{sw} = 0.7368$ m/s, $U_{so} = 0.7368$ m/s). (e) D O-in-W flow ($U_{sw} = 1.6579$ m/s, $U_{so} = 0.7368$ m/s).

III. MULTIVARIATE RECURRENCE NETWORK FROM TIME SERIES

Recurrence analysis is analyzing recurrence in phase space. For a given time series, we first need to reconstruct a phase space from the time series. In particular, when dealing with a time series $x(t)$ $(t = 1,2,...,N)$, we can use a suitable m-dimensional embedding with a proper time delay τ:

$$\vec{X}(t) = (x(t),x(t+\tau),\ldots,x[t+(m-1)\tau]),\quad t = 1,2,\ldots,N+m-1. \tag{1}$$

Given a certain threshold ε and a certain distance norm $\|\cdot\|$, we can get the recurrence relationship between any two space vectors:

$$R(i,j) = \Theta(\varepsilon - \| \vec{X}(i) - \vec{X}(j) \|), \tag{2}$$

where $\Theta(\cdot)$ is the Heaviside function and $\Theta(x) = \{1 \mid x > 0; 0 \mid x \leqslant 0\}$. The embedding dimension m and delay time τ should be properly selected to reconstruct phase space, and we use the False Nearest Neighbor (FNN) [59] method and C-C [60] method to determine m and τ, respectively. For more details about the recurrence analysis (recurrence plots), see the review paper by Marwan *et al.* [61]. We can interpret the recurrence matrix, Eq. (2), as an adjacency matrix of a complex network [34]:

$$A(i,j) = R(i,j) - \delta(i,j), \tag{3}$$

where $\delta(i,j)$ is the Kronecker delta introduced here in order to avoid artificial self-loops. Now this definition is extended to analyze four coupled dynamical time series (M_A, M_B, M_C, and M_D) from the same complex system. First, all four time series are embedded into the same phase space. For vectors that come from the same time series (such as M_A), the autorecurrence matrix is defined as follows:

$$R^A_{\text{auto}}(i,j) = \Theta(\varepsilon_A - \| \vec{M_A}(i) - \vec{M_A}(j) \|). \tag{4}$$

As for vectors from different time series (such as M_A and M_B), the cross-recurrence matrix can be defined as

$$R^{AB}_{\text{cross}}(i,j) = \Theta(\varepsilon_{AB} - \| \vec{M_A}(i) - \vec{M_B}(j) \|). \tag{5}$$

Combining the cross- and autorecurrence matrices, we can get an intersystem recurrence matrix, i.e., a multivariate recurrence matrix, as follows:

$$R_M = \begin{pmatrix} R^A_{\text{auto}} & R^{AB}_{\text{cross}} & R^{AC}_{\text{cross}} & R^{AD}_{\text{cross}} \\ R^{BA}_{\text{cross}} & R^B_{\text{auto}} & R^{BC}_{\text{cross}} & R^{BD}_{\text{cross}} \\ R^{CA}_{\text{cross}} & R^{CB}_{\text{cross}} & R^C_{\text{auto}} & R^{CD}_{\text{cross}} \\ R^{DA}_{\text{cross}} & R^{DB}_{\text{cross}} & R^{DC}_{\text{cross}} & R^D_{\text{auto}} \end{pmatrix}. \tag{6}$$

In order to consider R_M as a network of networks, the subnetwork $R_{\text{auto}}(\cdot)$ should be only weakly linked; i.e., the cross recurrences should be significantly lower than the autorecurrences:

$$\frac{1}{N(N-1)} \sum_{i \neq j} R^A_{\text{auto}}(i,j) > \frac{1}{N_A N_B} \sum_{i,j} R^{AB}_{\text{cross}}(i,j). \tag{7}$$

According to Ref. [58], we fix the auto- and cross-recurrence rate at 0.03 and 0.02, respectively. Note that the recurrence rate reflects the edge density of a recurrence network. For a time series, there exists a one to one mapping between the recurrence rate and the recurrence threshold, and one recurrence rate exclusively corresponds to one recurrence threshold. For different time series, the same recurrence rate can generate different recurrence thresholds. In particular, we determine the thresholds for autorecurrence (cross-recurrence) networks in terms of the same fixed autorecurrence (cross-recurrence) rate, and the recurrence thresholds for different autorecurrence (cross-recurrence) networks are different. Therefore, the thresholds in the multivariate recurrence matrix R_M can be different. Consequently, we obtain a multivariate recurrence network by interpreting the multivariate recurrence matrix as a network adjacent matrix. Mapping a multivariate time series into a recurrence network allows investigating of the dynamical characteristics of multivariate time series in terms of complex network theory.

IV. CHARACTERIZATION OF A MULTIVARIATE RECURRENCE NETWORK BY LOCAL CLUSTERING COEFFICIENTS

Based on the experimental signals measured from our four-sector conductance sensor, we construct multivariate recurrence networks for different horizontal oil-water flow patterns. In particular, representing the four signals from the four-sector conductance sensor through a corresponding recurrence network, we can then study the flow behavior from complex network analysis. Through analyzing the constructed networks, we find that all the multivariate recurrence networks exhibit the topological structure of a "network of networks." In order to characterize the local flow behavior from the structure of a network of networks, we employ the recently proposed local cross-clustering coefficient. A clustering coefficient of a node [62] quantifies how close its neighbors are to being a clique. Based on the definition of a clustering coefficient, a local clustering coefficient of a node v [37,40], denoted as $C^L(v)$, can be defined in terms of conditional probabilities as follows:

$$\begin{aligned} C^L(v) &= P(A(i,j) = 1 \mid A(v,i) = 1, A(v,j) = 1) \\ &= \frac{P(A(i,j) = 1, A(v,i) = 1, A(v,j) = 1)}{P(A(v,i) = 1, A(v,j) = 1)}, \end{aligned} \tag{8}$$

using Bayes's theorem, with

$$\begin{aligned} &P(A(v,i) = 1, A(v,j) = 1) \\ &\quad = \frac{1}{(N-1)(N-2)} \sum_{i=1}^{N} \sum_{j=1, j \neq i}^{N} A(v,i)A(v,j) \end{aligned} \tag{9}$$

and a similar expression for $P(A(i,j) = 1, A(v,i) = 1, A(v,j) = 1)$, where $A(i,j)$ is the adjacent matrix and N is the number of nodes in the complex network. For the recurrence network analysis of a single time series, the local clustering coefficient has been found to be an effective tool for uncovering the dynamic flow behavior underlying vertical upward bubbly oil in water flows [63]. More recently, a new concept of a local cross-clustering coefficient was derived from a local clustering coefficient [58,64]. For two subnetworks A and B, a local cross-clustering coefficient of node i in subnetwork A can be defined as follows:

$$C^{AB}_{\text{cross}}(i) = \begin{cases} \frac{\sum_{j \neq k} R^{AB}_{\text{cross}}(i,j) R^{AB}_{\text{cross}}(i,k) R^{B}_{\text{auto}}(j,k)}{k^{AB}_i (k^{AB}_i - 1)}, & k^{AB}_i \geqslant 2 \\ 0, & \text{else} \end{cases}, \tag{10}$$

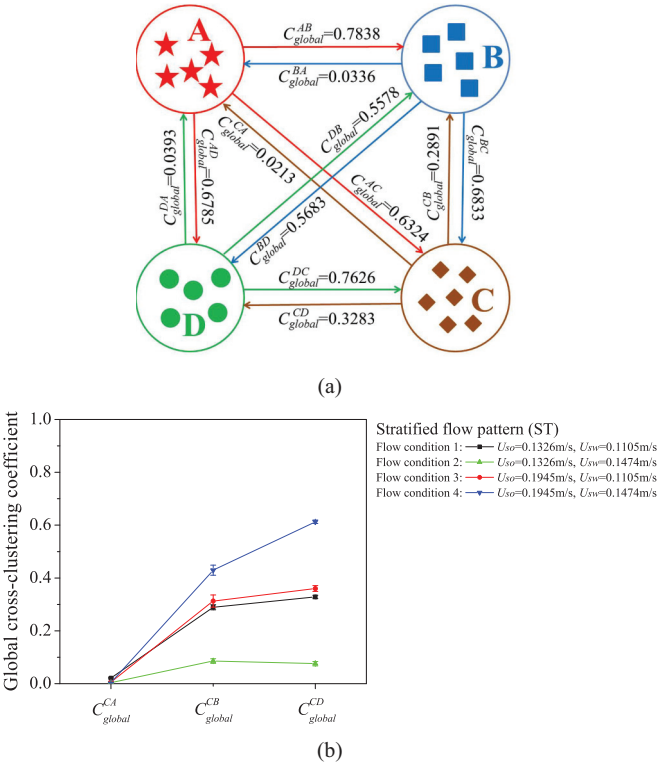

FIG. 6. (Color online) Global cross-clustering coefficients for the horizontal oil-water ST flow. (a) Cross-clustering coefficients of all pairs of subnetworks for the flow condition $U_{so} = 0.1326$ m/s, $U_{sw} = 0.1105$ m/s. (b) Distributions of C^{CA}_{global}, C^{CB}_{global}, and C^{CD}_{global} for different flow conditions, where the means and the standard deviations are presented.

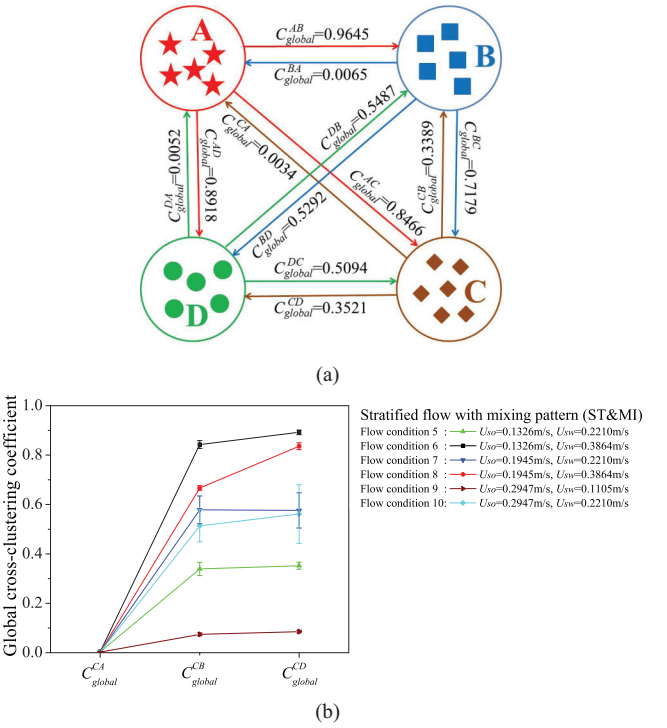

FIG. 7. (Color online) Global cross-clustering coefficients for the horizontal oil-water ST and MI flow. (a) Cross-clustering coefficients of all pairs of subnetworks for the flow condition $U_{so} = 0.1326$ m/s, $U_{sw} = 0.2210$ m/s. (b) Distributions of C^{CA}_{global}, C^{CB}_{global}, and C^{CD}_{global} for different flow conditions, where the means and the standard deviations are presented.

where $R_{cross}(i,j)$ is the cross-recurrence matrix, $R_{auto}(i,j)$ is the autorecurrence matrix, and ${k_i}^{AB}$ is the cross degree, i.e., the number of edges which connect node i with any node in subnetwork B. Actually, for node i belonging to subnetwork A, its local cross-clustering coefficient $C^{AB}_{cross}(i)$ estimates the probability that two randomly drawn neighbors of node i from subnetwork B are also neighbors. The global cross-clustering coefficient of subnetwork A is the average value of local cross-clustering coefficients over all N_A nodes in subnetwork A:

$$C^{AB}_{global} = \frac{1}{N_A}\sum_i C^{AB}_{cross}(i). \tag{11}$$

Next, this technique will be applied to our data.

V. APPLICATION TO CHARACTERIZE HORIZONTAL OIL-WATER FLOW PATTERNS

Four signals measured from one flow condition correspond to a multivariate recurrence network. It should be pointed out that the flow condition here refers to the flow behavior under different ratios between the water flow rate and the oil flow rate in a horizontal pipe. One flow condition corresponds to one certain flow pattern, but one flow pattern may include many different flow conditions. We totally construct 39 multivariate recurrence networks corresponding to five types of flow patterns from the experimental signals measured under 39 different flow conditions. For each generated multivariate recurrence network, there exist four subnetworks, denoted as subnetworks A, B, C, and D, resulting from the four different signals measured from the four sector sensor signals, M_A, M_B, M_C, and M_D, respectively. We calculate the global cross-clustering coefficients between all pairs of subnetworks for each constructed network to investigate the local flow behavior of different flow patterns. Note that, for each flow condition, we divide the four signals M_A, M_B, M_C, and M_D, into six parts with equal length, i.e., $M_A(i)$, $M_B(i)$, $M_C(i)$, $M_D(i)$, $i = 1,2,3,\ldots,6$. Then we construct the network and calculate the global cross-clustering coefficient for each part, and finally we obtain the ensemble mean and standard deviation of the global cross-clustering coefficients for the six parts (for one flow condition). Figures 6–8, 10, and 11 show ensemble means and standard deviations (error bars) of the global cross-clustering coefficients for the different flow conditions from ST flow, ST and MI flow, D O-in-W and W flow, D W-in-O and D O-in-W flow, and D O-in-W flow, respectively.

Figure 6 shows the distributions of global cross-clustering coefficients for the horizontal oil-water stratified flow (ST) pattern. Figure 6(a) shows the cross-clustering coefficients of all pairs of subnetworks for a flow condition $U_{so} = 0.1326$ m/s, $U_{sw} = 0.1105$ m/s. ST flow includes four different flow conditions, and, correspondingly, four multivariate recurrence networks are constructed and analyzed. Figure 6(b) presents the global cross-clustering coefficients for subnetwork C, i.e., for subnetwork C and $A(C^{CA}_{global})$, subnetwork C and

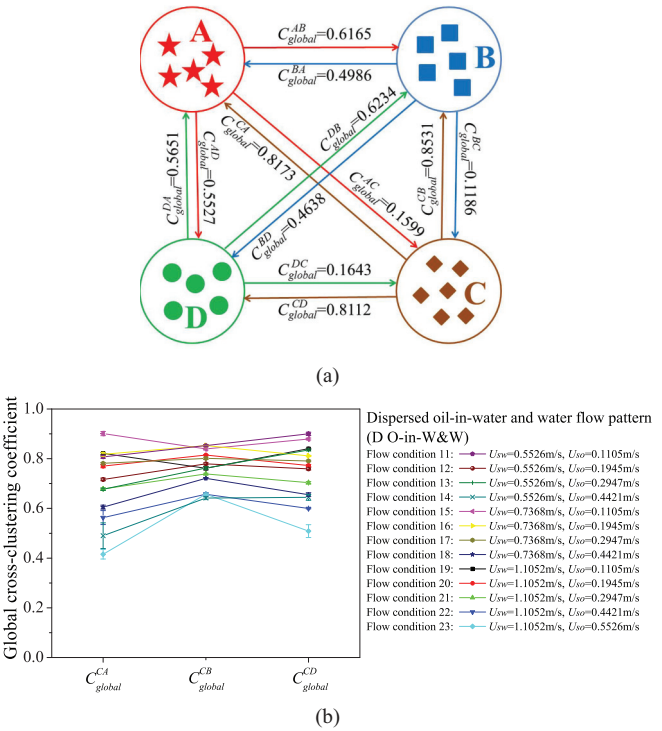

FIG. 8. (Color online) Global cross-clustering coefficients for the horizontal oil-water D O-in-W and W flow. (a) Cross-clustering coefficients of all pairs of subnetworks for the flow condition $U_{sw} = 0.7368$ m/s, $U_{so} = 0.1945$ m/s. (b) Distributions of C^{CA}_{global}, C^{CB}_{global}, and C^{CD}_{global} for different flow conditions, where the means and the standard deviations are presented.

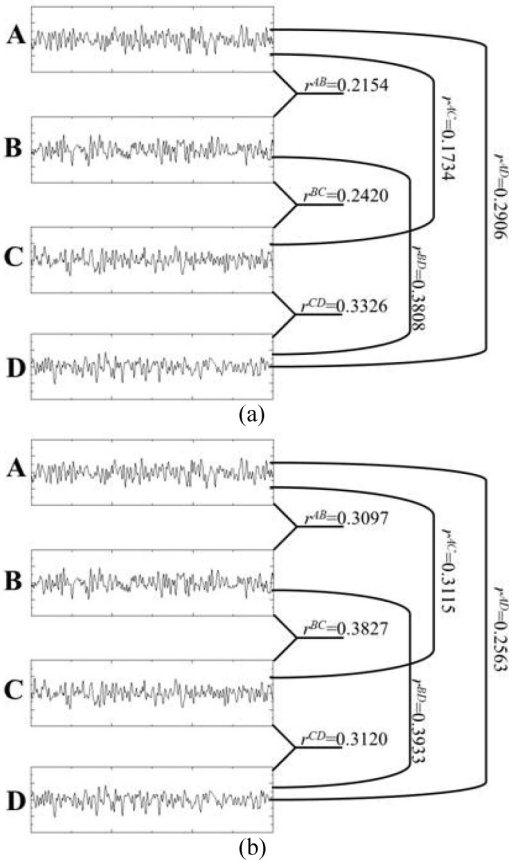

FIG. 9. Pearson correlation coefficient for the signals from the horizontal oil-water D O-in-W and W flow. (a) For the flow condition $U_{sw} = 0.7368$ m/s, $U_{so} = 0.1945$ m/s. (b) For the flow condition $U_{sw} = 0.7368$ m/s, $U_{so} = 0.4421$ m/s.

$B(C^{CB}_{global})$, and subnetwork C and $D(C^{CD}_{global})$. Similarly, in the Appendix, Figs. 14(a)–14(c) show the global cross-clustering coefficients for subnetworks A, B, and D, respectively. Note that subnetworks A, B, C, and D correspond to the signals measured from the upper, right, bottom, and left part of the pipe, as shown in Fig. 5. For the stratified flow, the upper part of the horizontal pipe is a continuous oil phase and the bottom part of the pipe is a continuous water phase. The ST flow pattern can be characterized by a smooth oil-water interface with no droplets and only small waves, as shown in Fig. 4(a). For the multivariate recurrence network from the ST flow pattern, subnetworks A and C reflect the flow behavior of continuous oil and water phases, respectively; subnetworks B and D reflect the interface fluctuation behavior. Note that the physical properties reflected by the cross-clustering coefficients are the local conductivity of the fluids. For example, if A is a nonconductive phase and C is a conductive phase, the global cross-clustering coefficient $C^{AC}_{global} > C^{CA}_{global}$. For the ST flow pattern, the conductivity of subnetwork A (continuous oil phase) is smaller than that of subnetworks B, C, and D, and the conductivity of subnetwork C (continuous water phase) is larger than that of subnetworks A, B, and D. Correspondingly, the global cross-clustering coefficients for A-B, A-C, and A-D are large and $C^{AB}_{global} > C^{BA}_{global}$, $C^{AC}_{global} > C^{CA}_{global}$, and $C^{AD}_{global} > C^{DA}_{global}$, as shown in Fig. 14(a) in the Appendix, while the global cross-clustering coefficients for C-A, C-B, and C-D are rather small, and $C^{CA}_{global} < C^{AC}_{global}$, $C^{CB}_{global} < C^{BC}_{global}$, and $C^{CD}_{global} < C^{DC}_{global}$, as shown in Fig. 6(b). The global cross-clustering coefficients for B-A and D-A are small and for B-C, B-D, D-B, and D-C are large, as shown in Figs. 14(b) and 14(c). In addition, we find that the global cross-clustering coefficient is very sensitive to the flow conditions. With an increase of the mixture flow rate, large amplitude fluctuations gradually appear on the oil-water interface and droplets in different size occur near the interface, indicating the onset of a stratified flow with mixing at interface pattern (ST and MI), as shown in Fig. 4(b). Figure 7 shows the distributions of global cross-clustering coefficients for the horizontal oil-water ST and MI flow pattern. Similar to the ST flow pattern, subnetwork A of the ST and MI pattern reflects the flow behavior of the continuous oil phase, and the global cross-clustering coefficients for A-B, A-C, and A-D are large, as shown in Fig. 15(a). In contrast to the ST flow pattern, there exist large amplitude interface fluctuations and a large number of droplets occurs near the interface. Correspondingly, the global cross-clustering coefficients for C-A are small but for C-B and C-D are large. Specifically, for a fixed oil flow rate, with an increase of the water flow rate, the global cross-clustering coefficients for B-C and B-D gradually decrease and C-B and C-D gradually increase; e.g., for a fixed $U_{so} = 0.1326$ m/s, U_{sw} increases from 0.2210 to 0.3864 m/s, as shown in Figs. 7(b) and 15(b), indicating the gradual appearance of

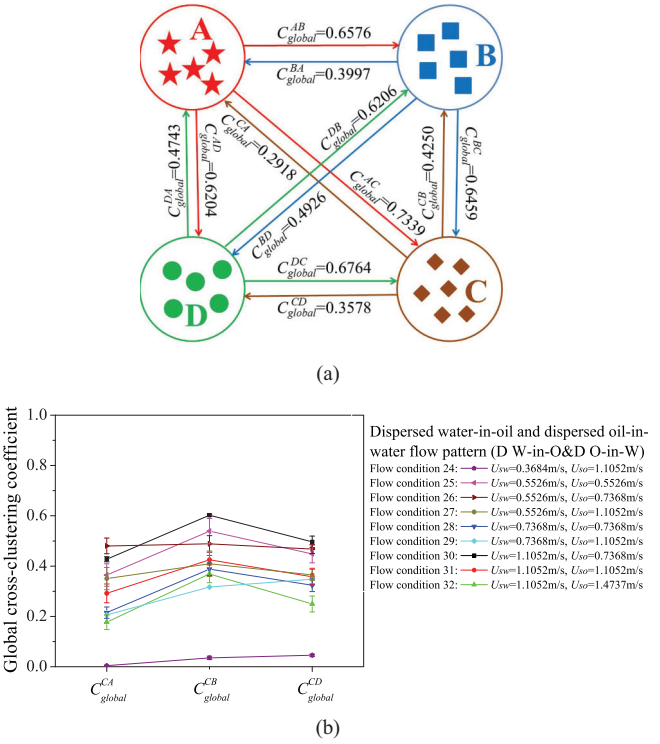

FIG. 10. (Color online) Global cross-clustering coefficients for the horizontal oil-water D W-in-O and D O-in-W flow. (a) Cross-clustering coefficients of all pairs of subnetworks for the flow condition $U_{sw} = 1.1052$ m/s, $U_{so} = 1.1052$ m/s. (b) Distributions of C^{CA}_{global}, C^{CB}_{global}, and C^{CD}_{global} for different flow conditions, where the means and the standard deviations are presented.

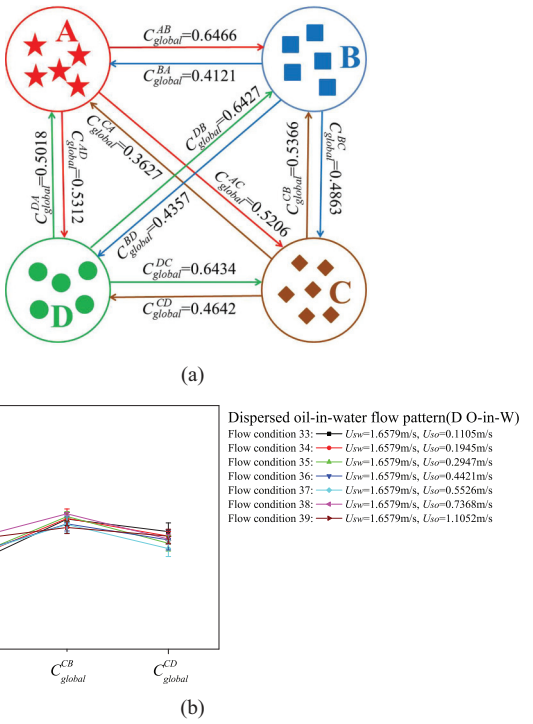

FIG. 11. (Color online) Global cross-clustering coefficients for the horizontal oil-water D O-in-W flow. (a) Cross-clustering coefficients of all pairs of subnetworks for the flow condition $U_{sw} = 1.6579$ m/s, $U_{so} = 0.1945$ m/s. (b) Distributions of C^{CA}_{global}, C^{CB}_{global}, and C^{CD}_{global} for different flow conditions, where the means and the standard deviations are presented.

droplets that are formed by a breakup of the interfacial waves induced by the increase of water flow rate. The droplets are still kept close to the interface, since neither of the phases contains sufficient energy to distribute the droplets across the pipe.

The stratified flow pattern (ST) and the stratified flow with mixing at interface pattern (ST and MI) belong to a segregated flow, where the oil and water are completely separated. With a further increase of the mixture flow rate, more and more liquid droplets appear on the oil-water interface. The hydrodynamics and buoyancy simultaneously work on the droplets. In particular, the hydrodynamics works as agitation to make the droplets distribute on the cross section of the pipe, while the buoyancy works against the descending trend induced by the gravity. With a gradual increase of liquid drops, the horizontal oil-water two-phase flow evolves from a stratified flow to a dispersed one. Dispersed flows are flows in which one phase is either fully or partially dispersed in the other. Depending on flow conditions, different dispersed flow patterns can appear there, such as a dispersion of oil in water and water flow pattern (D O-in-W and W), dispersion of water in oil and oil in water flow pattern (D W-in-O and D O-in-W), and dispersion of oil in water flow pattern (D O-in-W).

A D O-in-W and W flow pattern occurs at a high water flow rate and a middle oil flow rate. Figure 8 shows the distributions of global cross-clustering coefficients for a horizontal oil-water D O-in-W and W flow pattern. For the multivariate recurrence network from the D O-in-W and W flow pattern, subnetwork A reflects the flow behavior of dispersed oil droplets flowing in the water continuous phase and subnetwork C reflects the flow behavior of a water continuous phase; subnetworks B and D reflect the flow behavior associated with the number of dispersed oil droplets. Correspondingly, the global cross-clustering coefficients for A-B, A-D, C-A, C-B, and C-D are large while for A-C and B-C are small, as shown in Figs. 8(b) and 16(a)–16(c) in the Appendix. In addition, for a fixed water flow rate, with an increase of the oil flow rate, the global cross-clustering coefficients for C-A, C-B, and C-D gradually

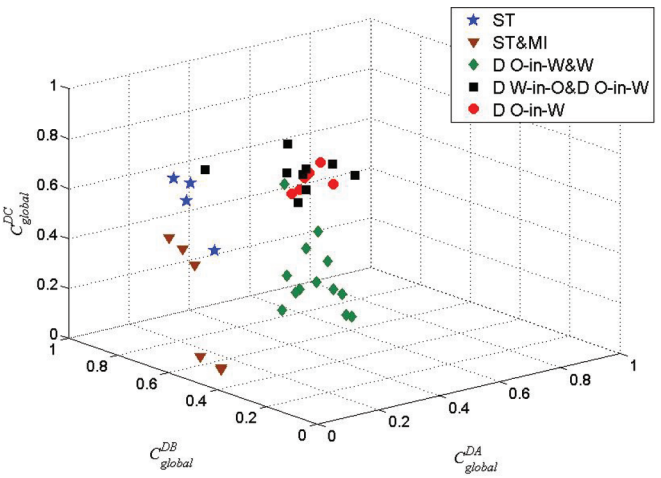

FIG. 12. (Color online) Joint distribution of C^{DA}_{global}, C^{DB}_{global}, and C^{DC}_{global} for different flow patterns.

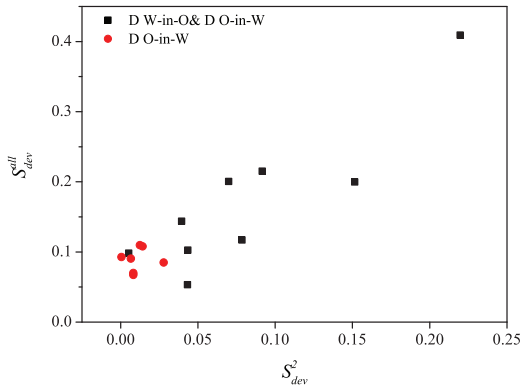

FIG. 13. (Color online) Joint distribution of $S^2_{\rm dev}$ and $S^{\rm all}_{\rm dev}$ for D W-in-O and D O-in-W and D O-in-W flow pattern. $S^2_{\rm dev}$ is the standard deviation of the cross-clustering coefficients $C^{DB}_{\rm global}$ and $C^{DC}_{\rm global}$; $S^{\rm all}_{\rm dev}$ is the standard deviation of the cross-clustering coefficients for all pairs of subnetworks.

decrease, as shown in Fig. 8(b), indicating intense movements of large numbers of oil droplets from the upper to the middle part of the horizontal pipe induced by an increase of the oil

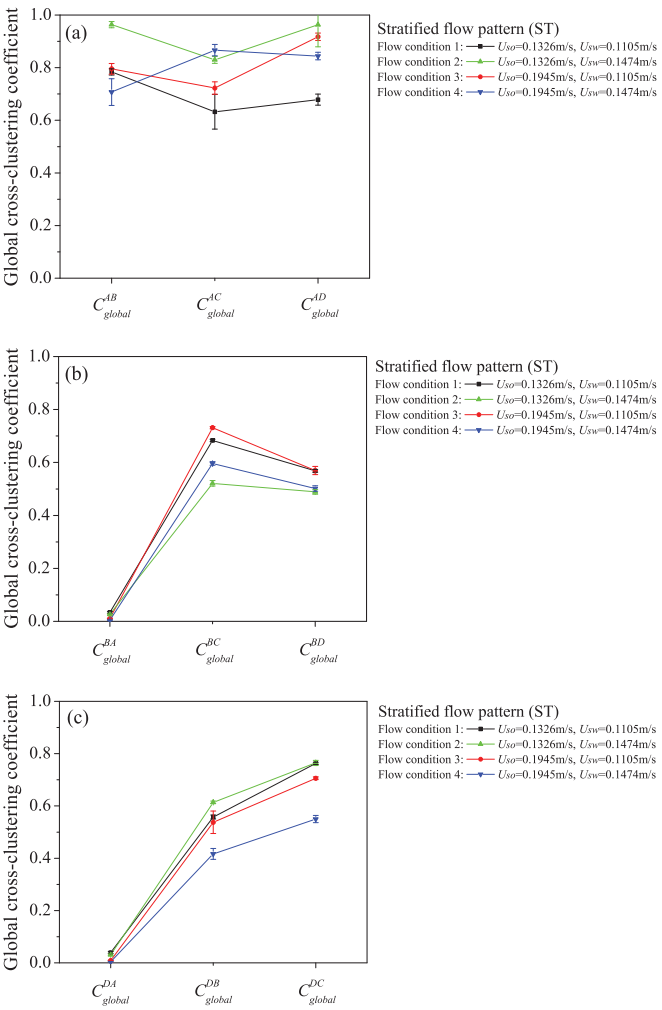

FIG. 14. (Color online) Distributions of global cross-clustering coefficients for the horizontal oil-water ST flow.

flow rate. For example, when the water flow rate is fixed at 0.7368 m/s, the global cross-clustering coefficients for C-A, C-B, and C-D gradually decrease from 0.9 to 0.6 as the oil flow rate increases from 0.1326 to 0.4421 m/s. Note that the Pearson correlation coefficient widely used in correlation analysis is infeasible to characterize the complex horizontal oil-water flow patterns. For example, we show the Pearson correlation coefficients for all pairs of signals for two different D O-in-W and W flow conditions in Fig. 9. For signals A and B, the Pearson correlation coefficient can be calculated as follows:

$$r^{AB} = \frac{\sum_{i=1}^{n}(A_i - \overline{A})(B_i - \overline{B})}{\sqrt{\sum_{i=1}^{n}(A_i - \overline{A})^2}\sqrt{\sum_{i=1}^{n}(B_i - \overline{B})^2}}. \qquad (12)$$

As can be seen, the Pearson correlation coefficients cannot clearly indicate the change of the flow condition and it is rather hard to extract an effective index to identify and characterize different flow behavior from the Pearson correlation analysis. Similar results can be observed for other flow patterns. In this regard, the Pearson correlation analysis does not allow uncovering of the flow behavior in the transitions of different horizontal oil-water flow conditions.

A D W-in-O and D O-in-W flow pattern occurs at a high water flow rate and a high oil flow rate. For the multivariate recurrence network from a D W-in-O and D O-in-W flow pattern, subnetwork A reflects the flow behavior of dispersed water droplets flowing in the oil continuous phase and subnetwork C reflects the flow behavior of oil droplets flowing in the water continuous phase; subnetworks B and D reflect the flow behavior associated with the number of dispersed water and oil droplets. Correspondingly, in contrast to a D O-in-W and W flow pattern, the global cross-clustering coefficients of D W-in-O and D O-in-W flow for A-B, A-C, A-D, and B-C are large while for C-A,C-B, and C-D are small, as shown in Figs. 10(b) and 17(a)–17(c). Furthermore, the global cross-clustering coefficients for C-A,C-B, and C-D are also very sensitive to the flow transition induced by an increase of the oil flow rate, as shown in Fig. 10(b). For example, when the water flow rate is fixed at 1.1052 m/s, the global cross-clustering coefficients for C-A,C-B, and C-D gradually decrease from 0.6 to 0.2 as the oil flow rate increases from 0.7368 to 1.4737 m/s. When the water flow rate is very high, the horizontal oil-water flow evolves into a D O-in-W flow pattern. For the multivariate recurrence network from a D O-in-W flow pattern, subnetworks A,B,C, and D all reflect the flow behavior of dispersed oil droplets flowing in the water continuous phase. Correspondingly, the distributions of global cross-clustering coefficients for a D O-in-W flow pattern are very concentrated, as shown in Fig. 11, which are quite different than distributions of other flow patterns.

To get a better visualization, we plot a three-dimensional figure for all flow conditions by regarding $C^{DA}_{\rm global}$, $C^{DB}_{\rm global}$, and $C^{DC}_{\rm global}$ without error bars as the x axis, y axis, and z axis, respectively, as shown in Fig. 12. As can be seen, except for the D W-in-O and D O-in-W and D O-in-W flow patterns, the global cross-clustering coefficients for different flow patterns are located in clearly distinct regions. For the D W-in-O and D O-in-W and D O-in-W flow patterns, we further extract two features from each flow condition: one is the

standard deviation of the global cross-clustering coefficients C^{DB}_{global} and C^{DC}_{global}, denoted as S^2_{dev}; the other is the standard deviation of the global cross-clustering coefficients for all pairs of subnetworks, denoted as $S^{\text{all}}_{\text{dev}}$. We plot these two extracted features in Fig. 13 and find that the two extracted standard deviations clearly allow us to distinguish a D W-in-O and D O-in-W flow pattern from a D O-in-W flow pattern. Note that there exists one overlapped point in Fig. 13 and this point corresponds to the flow condition at the transition from a D W-in-O and D O-in-W flow to a D O-in-W flow pattern. Therefore, the global cross-clustering coefficients can faithfully identify the distinct patterns of the horizontal oil-water two-phase flow. For example, when a transition in the flow pattern occurs, a characteristic change in the distributions of the global cross-clustering coefficients arises. These results suggest that cross clustering coefficients of a multivariate recurrence network is potentially a powerful tool for distinguishing different horizontal oil-water flow patterns and further allows for quantitatively uncovering the local flow behavior of the horizontal oil-water two-phase flow, a task that the existing method based on the Pearson correlation coefficient fails to achieve.

VI. CONCLUSIONS

Despite tremendous knowledge about multiphase flows, our understanding of horizontal oil-water flow patterns is still quite limited. We have designed a new multisector conductance sensor and systematically carried out horizontal oil-water two-phase flow experiments for measuring multivariate signals of different flow patterns. By applying the method of a multivariate recurrence network to multivariate experimental signals, we arrive at a result of a network of networks, which provides a new and powerful framework for characterizing local flow behavior underlying different horizontal oil-water flow patterns. Our results demonstrate that the cross-clustering coefficient of a multivariate recurrence network allows distinguishing of complex patterns arising from horizontal oil-water two-phase flow and can yield quantitative insights into the local flow behavior underlying different horizontal oil-water flow patterns. These results provide important clues for the prediction of pressure drop in the horizontal oil wells and measurement of flow parameters. These interesting findings render the multivariate recurrence network particularly powerful for investigating horizontal oil-water two-phase flow. This research provides an application of recurrence network theory in multivariate signal analysis and suggests that the multivariate recurrence network analysis allows identifying and characterizing of complex patterns of dynamical systems

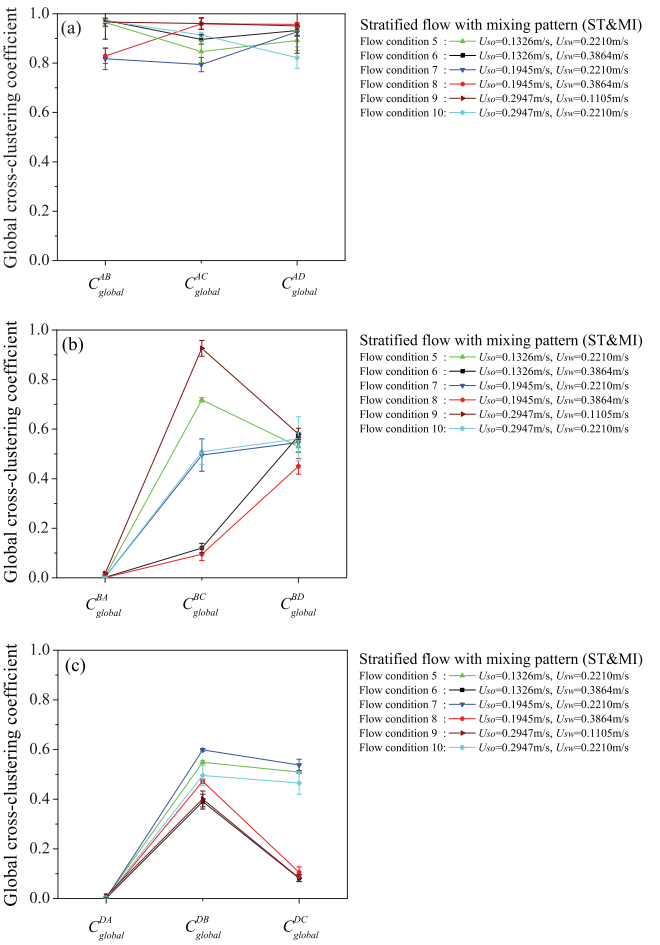

FIG. 15. (Color online) Distributions of global cross-clustering coefficients for the horizontal oil-water ST and MI flow.

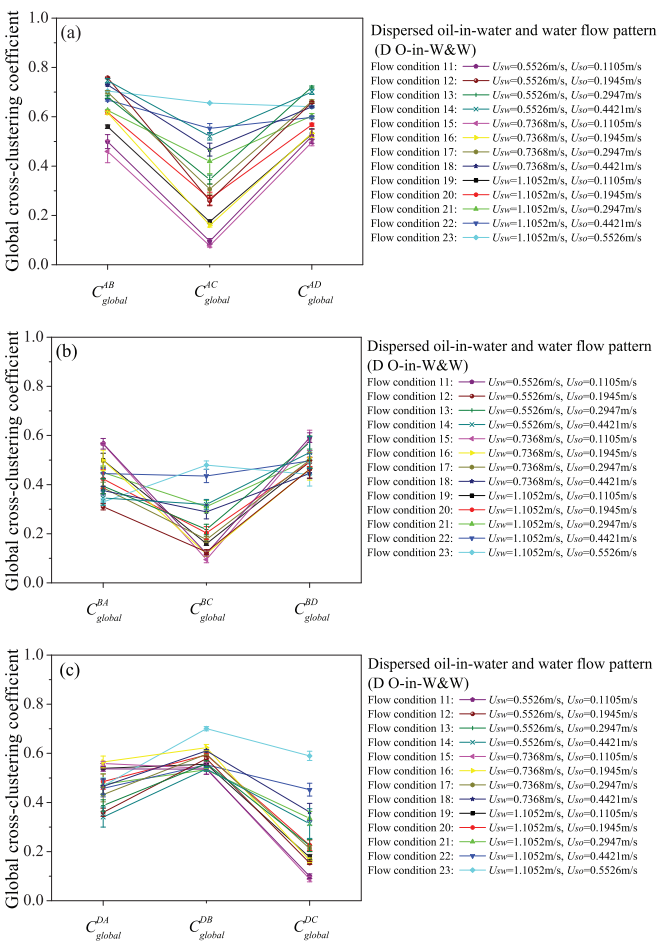

FIG. 16. (Color online) Distributions of global cross-clustering coefficients for the horizontal oil-water D O-in-W and W flow.

from experimental measurements, which makes a multivariate recurrence network a useful tool for the analysis of various complex systems from interdisciplinary research fields.

ACKNOWLEDGMENTS

Z. K. Gao was supported by National Natural Science Foundation of China under Grant No. 61104148, Specialized Research Fund for the Doctoral Program of Higher Education of China under Grant No. 20110032120088, Elite Scholar Program of Tianjin University, and Deutscher Akademischer Austauschdienst Foundation. N. D. Jin was supported by National Natural Science Foundation of China under Grant No. 41174109 and National Science and Technology Major Project of China under Grant No. 2011ZX05020-006. J. Kurths was supported by International Research Training Group (IRTG) 1740 (Deutsche Forschungsgemeinschaft).

APPENDIX

There are 39 flow conditions corresponding to five different flow patterns. We calculate 12 different cross-clustering coefficients for each flow conditions. Three global cross-clustering coefficients, i.e., C^{CA}_{global}, C^{CB}_{global}, and C^{CD}_{global}, are shown in the main text, and the other 12 cross-clustering coefficients are shown in the Appendix. Note that the in the construction of a multivariate recurrence network the embedding dimension m and the delay time τ are determined by the FNN [59] method and the C-C [60] method (two standard methods), respectively. Specifically, for the stratified flow pattern (ST) $m = 3$ and $\tau = 18$; for the stratified flow with mixing at an interface pattern (ST and MI) $m = 3$ and $\tau = 24$; for the dispersion of oil in water and water flow pattern (D O-in-W and W) $m = 3$ and $\tau = 10$; for the dispersion of water in oil and oil in water flow pattern (D W-in-O and D O-in-W) $m = 3$ and $\tau = 11$; for the dispersion of oil in water flow pattern (D O-in-W) $m = 3$ and $\tau = 17$. Figures 14–18 show the distributions of global cross-clustering coefficients for the horizontal oil-water ST flow, ST and MI flow, D O-in-W and W flow, D W-in-O and D O-in-W flow, and D O-in-W flow, respectively. As can be seen from Fig. 14, for the ST flow, the global cross-clustering coefficients for *B-A* and *D-A* are small, and for *B-C*, *B-D*, *D-B*, and *D-C* they are large. We can see from Fig. 15, for the ST and MI flow, for a fixed oil flow rate, with an increase of the water flow rate, the global cross-clustering coefficients for *B-C* and *B-D* gradually decrease; e.g., for a fixed $U_{\text{so}} = 0.1326$ m/s, U_{sw} increases from 0.2210 to 0.3864 m/s, indicating the gradual appearance of droplets that are formed by a breakup of the interfacial waves induced by the increase of the water flow

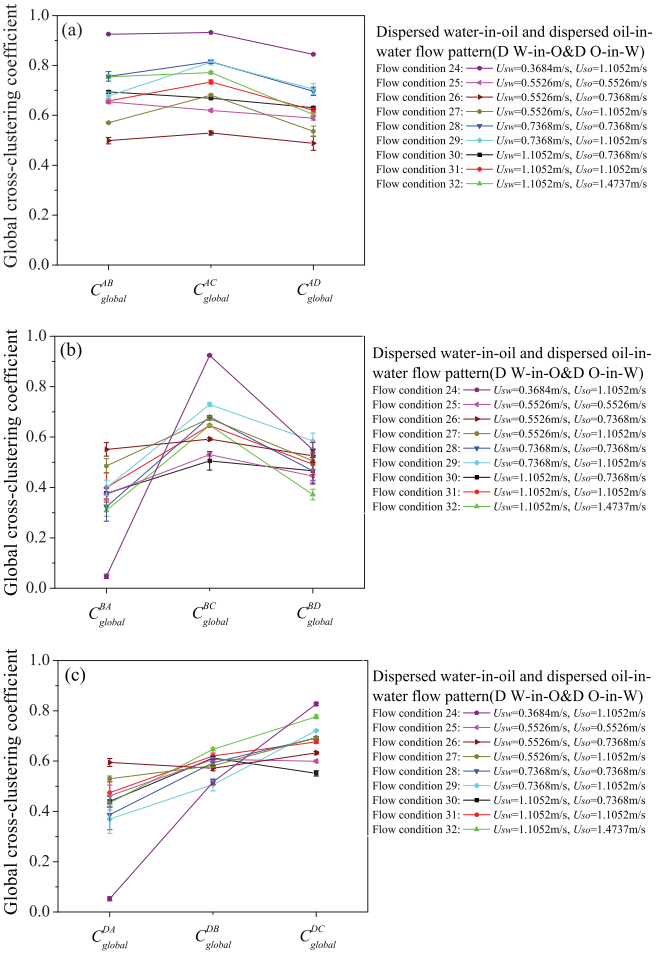

FIG. 17. (Color online) Distributions of global cross-clustering coefficients for the horizontal oil-water D W-in-O and D O-in-W flow.

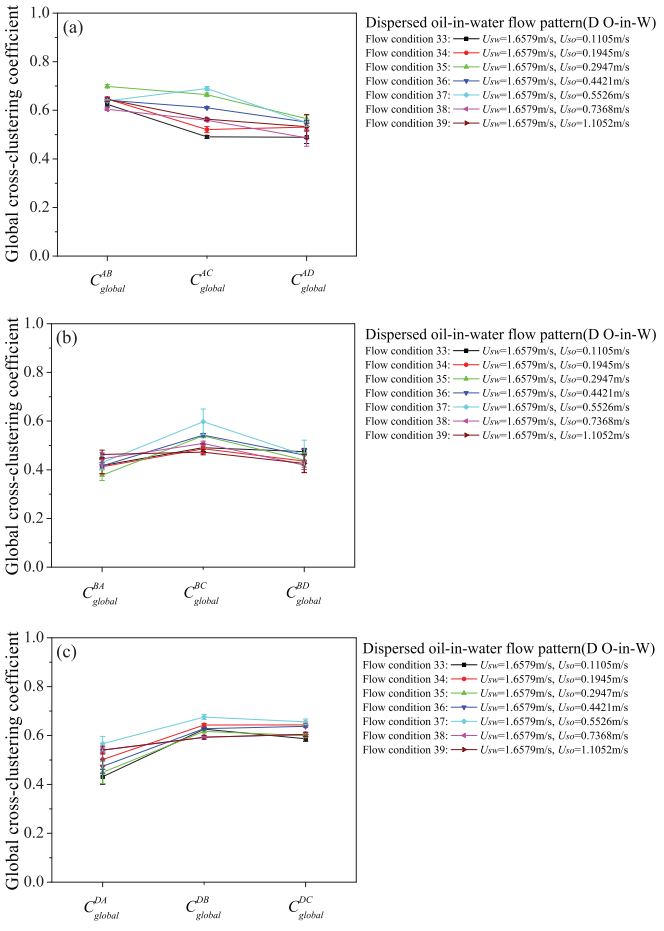

FIG. 18. (Color online) Distributions of global cross-clustering coefficients for the horizontal oil-water D O-in-W flow.

rate. For the D O-in-W and W flow, the global cross clustering coefficients for A-B and A-D are large, while for A-C and B-C they are small, as shown in Fig. 16. In contrast to a D O-in-W and W flow pattern, the global cross-clustering coefficients of D W-in-O and D O-in-W flow for A-B, A-C, A-D, and B-C are large, as shown in Fig. 17. As can be seen from Fig. 18, the distributions of global cross-clustering coefficients for D O-in-W flow are very concentrated, indicating that all subnetworks reflect the same flow behavior of dispersed oil droplets flowing in the water continuous phase.

[1] J. L. Trallero, C. Sarica, and J. P. Brill, SPE Production and Facilities **12**, 165 (1997).
[2] P. Angeli and G. F. Hewitt, Int. J. Multiphase Flow **26**, 1117 (2000).
[3] T. S. Ng, C. J. Lawrence, and G. F. Hewitt, Int. J. Multiphase Flow **27**, 1301 (2001).
[4] N. Brauner and A. Ullmann, Int. J. Multiphase Flow **28**, 1177 (2002).
[5] D. P. Chakrabarti, G. Das, and P. K. Das, AIChE J. **52**, 3668 (2006).
[6] K. Piela, R. Delfos, G. Ooms, J. Westerweel, and R. V. A. Oliemans, Int. J. Multiphase Flow **34**, 665 (2008).
[7] W. A. S. Kumara, B. M. Halvorsen, and M. C. Melaaen, Chem. Eng. Sci. **65**, 4332 (2010).
[8] T. Al-Wahaibi and P. Angeli, Chem. Eng. Sci. **62**, 2915 (2007).
[9] T. Al-Wahaibi and P. Angeli, Int. J. Multiphase Flow **37**, 930 (2011).
[10] R. G. Morgan, C. N. Markides, C. P. Hale, and G. F. Hewit, Int. J. Multiphase Flow **43**, 101 (2012).
[11] S. M. Pincus, Proc. Natl. Acad. Sci. USA **88**, 2297 (1991).
[12] D. L. Jones and R. G. Baraniuk, IEEE Transactions on Signal Processing **43**, 2361 (1995).
[13] M. Du, N. D. Jin, Z. K. Gao, and B. Sun, Chem. Eng. Sci. **82**, 144 (2012).
[14] C. Zhou and J. Kurths, Phys. Rev. Lett. **96**, 164102 (2006).
[15] S. Boccaletti, V. Latora, Y. Moreno, M. Chavez, and D. U. Hwang, Physics Reports **424**, 175 (2006).
[16] L. Huang, K. Park, Y. C. Lai, L. Yang, and K. Q. Yang, Phys. Rev. Lett. **97**, 164101 (2006).
[17] J. Nawrath, M. C. Romano, M. Thiel, I. Z. Kiss, M. Wickramasinghe, J. Timmer, J. Kurths, and B. Schelter, Phys. Rev. Lett. **104**, 038701 (2010).
[18] S. V. Buldyrev, R. Parshani, G. Paul, H. E. Stanley, and S. Havlin, Nature (London) **464**, 1025 (2010).
[19] G. Ansmann and K. Lehnertz, Phys. Rev. E **84**, 026103 (2011).
[20] J. Gao, S. V. Buldyrev, H. E. Stanley, and S. Havlin, Nature Physics **8**, 40 (2012).
[21] A. Rothkegel and K. Lehnertz, Chaos **22**, 013125 (2012).
[22] K. Iwayama, Y. Hirata, K. Takahashi, K. Watanabe, K. Aihara, and H. Suzuki, Scientific Reports **2**, 423 (2012).
[23] G. A. Mendes, L. R. da Silva, and H. J. Herrmann, Physica A **391**, 362 (2012).
[24] G. L. Mamede, N. A. M. Arajo, C. M. Schneider, J. C. de Arajo, and H. J. Herrmann, Proc. Natl. Acad. Sci. USA **109**, 7191 (2012).
[25] P. Menck, J. Heitzig, N. Marwan, and J. Kurths, Nature Physics **9**, 89 (2013).
[26] J. Zhang and M. Small, Phys. Rev. Lett. **96**, 238701 (2006).
[27] J. Zhang, J. Sun, X. Luo, K. Zhang, T. Nakamura, and M. Small, Physica D **237**, 2856 (2008).
[28] Y. Yang and H. J. Yang, Physica A **387**, 1381 (2008).
[29] L. Lacasa, B. Luque, F. Ballesteros, J. Luque, and J. C. Nuno, Proc. Natl. Acad. Sci. USA **105**, 4972 (2008).
[30] L. Lacasa and R. Toral, Phys. Rev. E **82**, 036120 (2010).
[31] C. Liu, W. X. Zhou, and W. K. Yuan, Physica A **389**, 2675 (2010).
[32] Y. Shimada, T. Ikeguchi, and T. Shigehara, Phys. Rev. Lett. **109**, 158701 (2012).
[33] X. Xu, J. Zhang, and M. Small, Proc. Natl. Acad. Sci. USA **105**, 19601 (2008).
[34] N. Marwan, J. F. Donges, Y. Zou, R. V. Donner, and J. Kurths, Phys. Lett. A **373**, 4246 (2009).
[35] Z. K. Gao and N. D. Jin, Chaos **19**, 033137 (2009).
[36] Z. K. Gao and N. D. Jin, Phys. Rev. E **79**, 066303 (2009).
[37] R. V. Donner, Y. Zou, J. F. Donges, N. Marwan, and J. Kurths, New J. Phys. **12**, 033025 (2010).
[38] R. V. Donner, J. Heitzig, J. F. Donges, Y. Zou, N. Marwan, and J. Kurths, Eur. Phys. J. B **84**, 653 (2011).
[39] R. V. Donner, M. Small, J. F. Donges, N. Marwan, Y. Zou, R. Xiang, and J. Kurths, Int. J. Bifurcation Chaos **21**, 1019 (2011).
[40] J. F. Donges, J. Heitzig, R. V. Donner, and J. Kurths, Phys. Rev. E **85**, 046105 (2012).
[41] Y. Dong, W. W. Huang, and Z. H. Liu, Physica A **392**, 967 (2013).
[42] W. X. Wang, R. Yang, Y. C. Lai, V. Kovanis, and C. Grebogi, Phys. Rev. Lett. **106**, 154101 (2011).
[43] W. X. Wang, R. Yang, Y. C. Lai, V. Kovanis, and M. A. F. Harrison, Europhys. Lett. **94**, 48006 (2011).
[44] D. M. Song, Z. Q. Jiang, and W. X. Zhou, Physica A **388**, 2450 (2009).
[45] M. C. Qian, Z. Q. Jiang, and W. X. Zhou, J. Phys. A: Math. Theor. **43**, 335002 (2010).
[46] J. F. Donges, Y. Zou, N. Marwan, and J. Kurths, Europhys. Lett. **87**, 48007 (2009).
[47] J. F. Donges, R. V. Donner, M. H. Trauth, N. Marwan, H. J. Schellnhuber, and J. Kurths, Proc. Natl. Acad. Sci. USA **108**, 20422 (2011).
[48] J. Zhang, K. Zhang, J. F. Feng, and M. Small, PLoS Comput. Biol. **6**, e1001033 (2010).
[49] M. Chavez, M. Valencia, V. Navarro, V. Latora, and J. Martinerie, Phys. Rev. Lett. **104**, 118701 (2010).
[50] S. Hempel, A. Koseska, J. Kurths, and Z. Nikoloski, Phys. Rev. Lett. **107**, 054101 (2011).
[51] X. Li and Z. Dong, Phys. Rev. E **84**, 062901 (2011).
[52] Z. K. Gao, N. D. Jin, W. X. Wang, and Y. C. Lai, Phys. Rev. E **82**, 016210 (2010).
[53] Z. K. Gao and N. D. Jin, Chem. Eng. Sci. **66**, 2660 (2011).
[54] D. M. Walker and A. Tordesillas, Phys. Rev. E **85**, 011304 (2012).

[55] D. M. Walker, A. Tordesillas, S. Pucilowski, Q. Lin, A. L. Rechenmacher, and S. Abedi, Int. J. Bifurcation Chaos **22**, 1230042 (2012).
[56] H. O. Ghaffari and R. P. Young, Nonlinear Processes Geophys. **19**, 215 (2012).
[57] H. O. Ghaffari and R. P. Young, Europhys. Lett. **98**, 48003 (2012).
[58] J. H. Feldhoff, R. V. Donner, J. F. Donges, N. Marwan, and J. Kurths, Phys. Lett. A **376**, 3504 (2012).
[59] M. B. Kennel, R. Brown, and H. D. I. Abarbanel, Phys. Rev. A **45**, 3403 (1992).
[60] H. S. Kim, R. Eykholt, and J. D. Salas, Physica D **127**, 48 (1999).
[61] N. Marwan, M. C. Romano, M. Thiel, and J. Kurths, Phys. Rep. **438**, 237 (2007).
[62] D. J. Watts and S. H. Strogatz, Nature (London) **393**, 440 (1998).
[63] Z. K. Gao, X. W. Zhang, M. Du, and N. D. Jin, Phys. Lett. A **377**, 457 (2013).
[64] J. F. Donges, H. C. H. Schultz, N. Marwan, Y. Zou, and J. Kurths, Eur. Phys. J. B **84**, 635 (2011).